IEEE Robotics and Automation Letters (RA-L) paper, presented at ICRA 2023, London, UK. Cite as RA-L paper.

Modeling and Characterizing Two Dielectric Elastomer Folding Actuators for Origami-inspired Robot

Yang Li, and Ting Zhang*, *Member, IEEE*

***Abstract*—Origami-inspired robots are automated machines that achieve deformation and function through folding. This letter models and characterizes two dielectric elastomer folding actuators, and proposes a new method for driving origami-inspired robots. Multilayer bending dielectric elastomer actuators (MBDEAs) and minimum energy structural dielectric elastomer actuators (MESDEAs) are placed at the creases to drive a rigid origami-inspired robot joint. We establish an analytical model of MBDEAs based on beam bending theory. This model establishes the relationships between the deformation angle and output moment of the MBDEA and the input electric field intensity according to the design parameters. In addition, a design model of MESDEAs with the rectangular hollow area is presented for the equilibrium deformation angle and maximum output moment. The analytical model of MBDEAs for the deformation angle and the design model of MESDEAs are both preliminarily verified by experiments. Finally, we realize the drive of the joint based on MBDEAs and MESDEAs. The design and model are evaluated through experiments. This work paves the way for subsequent motion control of origami-inspired robots and further expands the application fields of dielectric elastomer actuators (DEAs).**

***Index Terms*—Origami-inspired robots, multilayer bending dielectric elastomer actuators, minimum energy structural dielectric elastomer actuators, dielectric elastomer actuators.**

I. Introduction

ORIGAMI-INSPIRED robots have shown great prospects in service, medical treatment, space exploration, and other fields [1]. Origami-inspired robots are automated machines that achieve deformation and function through folding. The origami-inspired robot transformed from two-dimensional sheets into three-dimensional structures through folding joints. And the three-dimensional origami structures can be reconfigured by programming, and volumetrically changed from resting state to various desired shapes [2]. Origami folding joints, called hinges, are very important for origami-inspired robots and determine the movability and the build-in compliance of the origami-inspired robot [3]. The shape changes of the origami-inspired robot are determined by the folding pattern and embedded actuators. Many actuators have been used in origami-inspired robots, such as pneumatic [4]-[7], magnetic [8]-[11], cable [12]-[15], and active materials [8], [16]-[20].

Self-actuating origami-inspired robots driven by smart materials, such as electroactive polymers (EAPs), shape memory alloys (SMAs) or shape memory polymers (SMPs), have simple structures and flexible deformation. Combining origami structures with smart materials can make full use of their advantages, realize the conversion of origami structures from "folded" to "self-folded" and make the deformation of origami-inspired robots more "intelligent". Most existing studies apply thermal-active materials to origami folding joints. However, it is difficult to control the temperature field quickly and accurately, and there are efficiency problems in the heating and cooling process, which obviously limits the application of origami-inspired robots. Dielectric elastomer (DE), a kind of EAP, can produces deformation under the electric field. Compared with other smart materials like SMA, SMP and conductive films, DEs have many advantages such as large deformation, rapid response and their working conditions are easy to achieve [21]. Therefore, they show great prospects in driving origami-inspired robots. However, there are few studies on applying DEs to origami-inspired robots. Generally, a dielectric elastomer actuator (DEA) consists of a DE film with compliant electrodes covering on both sides. When an electric field works on the compliant electrodes, the DE film will compress in thickness and extend in plane [22]. According to DEA's actuation principle, various actuators have been made [23]-[31]. Among them, DEAs based on multilayered unimorph and minimum energy structure do not need rigid support, are simple to fabricate and can achieve folding motion, so they are more suitable for folding hinges.

In this letter, DEAs based on multilayered unimorph and minimum energy structure are called multilayer bending dielectric elastomer actuators (MBDEAs) and minimum energy structural dielectric elastomer actuators (MESDEAs), respectively. The deformation angle and output moment are two important performance indicators of actuators, especially in the driving aspect of origami-inspired robots. The deformation angle and output moment of MBDEAs and MESDEAs are related to many of their design parameters, so it is necessary to investigate the design methods for both DEAs.

Manuscript received: May 7, 2022; Revised: July 19, 2022; Accepted: August 18, 2022.

This paper was recommended for publication by Editor Cecilia Laschi upon evaluation of the Associate Editor and Reviewers' comments. This work was supported in part by the National Key R&D Program of China (2020YFC2007804), the Natural Science Foundation of the Jiangsu Higher Education Institutions of China (19KJA180009), the Natural Science Foundation of Jiangsu Province (BK20191424), the Jiangsu Frontier Leading Technology Fundamental Research Project (BK20192004D), and the Distinguished Professor of Jiangsu province. (*Corresponding author: Ting Zhang*)

Yang Li and Ting Zhang are with the Robotics and Microsystems Center, College of Mechanical and Electrical Engineering, Soochow University, Suzhou 215000, China. (e-mail: zhangt.hit@gmail.com).

* Corresponding authors

Digital Object Identifier (DOI): see top of this page.

Balakrisnan *et al*. applied the model developed by Devoe *et al*. [32] to EAP-based bending actuators with at most two active layers [33]. The model did not consider the DE material's electromechanical response or the effect of the number of active layers on actuator's performance. Ahmed *et al*. developed sets of nondimensional expressions for curvature, displacement at the tip and blocked force induced by the electric field, considering various design parameters (thickness, layers' number, Young's modulus, and electric field intensity, etc.) to guide the experimental design and fabrication of multilayered EAP actuators, and used P(VDF–TrFE–CTFE) to verify the analytical model by experiments [18]. Kai *et al*. presented a multilayer membrane element based on absolute nodal coordinate formulation for multilayer DEAs' dynamic modeling, considering the coupling of rigid-body motion and large deformation to the electric field [34]. In addition, O'Brien *et al*. used a hybrid Arruda–Boyce strain energy function to characterize DEMES behavior [35], [36]. Rosset *et al*. used the minimum energy principle (sum of DE film's strain energy, the electrostatic energy and the frame's bending energy) to model and design a MESDEA [37]. Above models [34]-[37] all used energy density equations of hyperelastic materials to characterize DE's constitutive behaviors. However, it is difficult to accurately measure the mechanical parameters in energy density equations due to DE's viscoelasticity. Wang *et al*. proposed that DE film's moment to the elastic frame is proportional to its volume in the hollow area and verified it, then presented a design method of MESDEAs with the double semicircular hollow area [38].

Here, two dielectric elastomer folding actuators namely MBDEAs and MESDEAs, are modeled and characterized for origami-inspired robots. And DEAs are integrated for the first time to drive a rigid origami-inspired robot joint. We establish an analytical model of the MBDEA's deformation angle and output moment and use VHB F9473PC for experimental verification. In addition, a design model of MESDEAs with rectangular hollow areas for the equilibrium deformation angle and maximum output moment is presented.

II. Modeling

A. Origami-inspired Robot Joint

To explore the application potential of DEAs in origami-inspired robots, we select a rigid origami-inspired robot joint for experimentation. Fig. 1 shows the structure of the joint which is composed of two sheets and three legs. The folding sheets can be made from 3D-printed resin or laser-cut plastic sheets, with soft materials such as silicone at the creases. The joint can produce telescopic and bending deformation, and has three degrees of freedom, as shown in Fig. 1.

Fig. 2 shows the prototype of the origami-inspired robot joint. The crease together with its adjacent hexagonal sheet and pentagonal sheet is defined as an origami folding hinge in this letter. The telescopic displacement and bending angle of the joint depend on the three legs. To control the deformation of the joint, we use MBDEAs and MESDEAs placed at the creases to directly drive the origami folding hinges, as shown in Fig. 2. The folding sheets are made by 3D printing with a thickness of 0.7 mm. The side length a of the two hexagonal sheets and the length l of the legs' pentagonal sheets are both 50 mm. The six sheets of each leg are connected by tapes, and the three legs are connected with the two hexagonal sheets by shrink films. The joint is initially elongated. Besides, the driving voltage of DE is large (kV level), so a high voltage power supply (EMCO Q101-5) is used to connect the compliant electrodes.

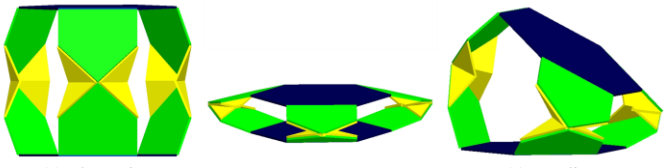

Fig. 1. Three states of the origami-inspired robot joint.

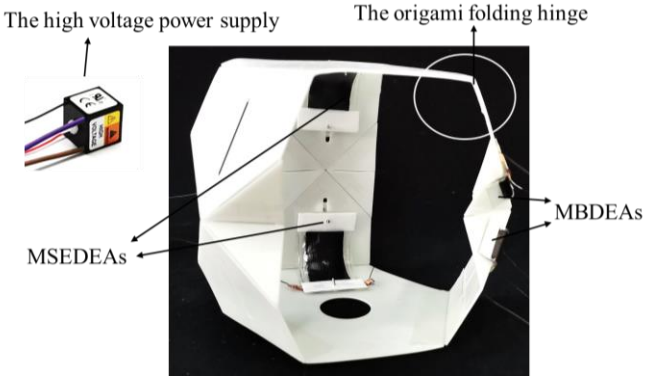

Fig. 2. The DEAs driven Origami-inspired robot joint.

B. Modeling of MBDEAs

1) Working Principle of MBDEAs

The MBDEA consists of active and passive layers. The role of the passive layer is to hinder the deformation of the active layer when it intends to stretch under an electric field. And the strain imbalance will result in MBDEA's bending deformation, as shown in Fig. 3(a). The active layer is one layer of DE film with compliant electrodes covering on both sides and the passive layer is also a flexible material (such as PDMS, scotch tape, or DE without covering electrodes, etc.). The deformation angle and output moment of the MBDEA depend on many factors, including: the type, size and number of layers of the DE and passive layer.

2) Analytical model of MBDEAs

The analytical model of MBDEAs is based on beam bending theory and considers the nonlinear relationship between the induced stress and the applied electric field. The multilayer system includes passive layers and DEs, and the electrodes are ignored because of their small thickness. The section of the MBDEA is shown in Fig. 3(b). When the MBDEA bends, the relationship between strain ε and height y is:

$$\varepsilon(y) = \varepsilon_0' + \frac{y}{\rho} = \varepsilon_0' + y\kappa;\ -t_p \le y \le h_n \tag{1}$$

where $\varepsilon(y)$ represents the strain at height y, ε_0' is the strain when y=0, ρ is MBDEA's curvature radius, κ is MBDEA's curvature, t_p is the thickness of the passive layer, and $h_n = nt_a$ is n-layer DEs' height. For the passive layer,

$$\sigma_p = Y_p\varepsilon_p = Y_p(\varepsilon_0' + y\kappa);\ -t_p \le y \le 0 \tag{2}$$

where Y_p is the elastic modulus of the passive layer, σ_p is the normal stress on the passive layer's section. Also, the normal stress on the section of DE is:

$$\sigma_a = Y_a(\varepsilon_0{}' + y\kappa - M_a E^2);\ 0 \le y \le h_n \quad (3)$$

$$M_a = \frac{\mu\varepsilon_0\varepsilon_r}{Y_a} \quad (4)$$

where σ_a is the normal stress on the section, Y_a is DE's elastic modulus, M_a is DE's electrostrictive coefficient [39], which is calculated by (4), μ is DE's Poisson's ratio, ε_0 is the permittivity in vacuum with the value of 8.854×10^{-12} F/m, and ε_r is DE's relative permittivity which depends on the type of material. When there is no external force or moment applying to the MBDEA, its resultant force and moment are both zero:

$$\int_{-t_p}^{h_n} \sigma\, dA = 0 \Longrightarrow \int_{-t_p}^{0} \sigma_p dA + \int_{0}^{h_n} \sigma_a dA = 0 \quad (5)$$

$$\int_{-t_p}^{h_n} \sigma y\, dA = 0 \Longrightarrow \int_{-t_p}^{0} \sigma_p y dA + \int_{0}^{h_n} \sigma_a y dA = 0 \quad (6)$$

Substituting (2) and (3) into (5) and (6), then the expression of κ is obtained:

$$\kappa = \left[\frac{6n\alpha\beta(n+\alpha)}{4n\alpha^3\beta+4n^3\alpha\beta+\alpha^4\beta^2+n^4+6n^2\alpha^2\beta}\right]\frac{M_a E^2}{t_a} \quad (7)$$

where n is the number of layers of DE, $\alpha = \frac{t_p}{t_a}$, $\beta = \frac{Y_p}{Y_a}$, E is the external applied electric field intensity and its relationship with voltage V is $E = \frac{V}{t_a}$, and t_a is the thickness of the DE.

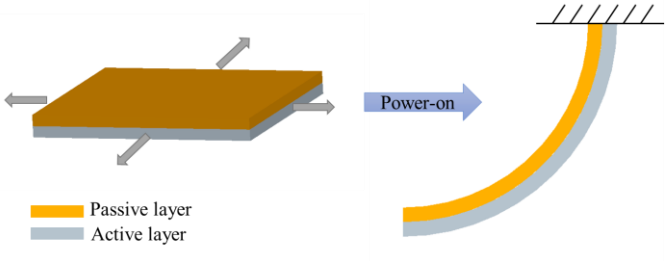

(a) Bending principle

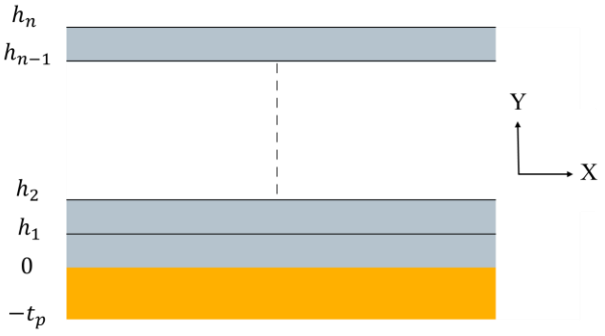

(b) Section diagram

Fig. 3. MBDEA's bending principle and section diagram.

Then the deformation angle θ at the end of the MBDEA is:

$$\theta = \kappa L \quad (8)$$

where L is the length of the MBDEA. Regarding the MBDEA as a purely curved beam, the electric field applied to the MBDEA can be converted into an equivalent bending moment, so the output moment of the MBDEA is,

$$M = \frac{YI}{\rho} = YI\kappa \quad (9)$$

where YI is MBDEA's equivalent bending stiffness,

$$YI = b\int_{-\frac{h}{2}}^{\frac{h}{2}} Y(y)y^2 dy = \frac{bY_a t_a{}^3}{3}\left(\frac{n^3+3n\alpha^2+\alpha^3\beta+3n^2\alpha\beta}{4}\right)$$

where b is MBDEA's width.

Note that some assumptions are made when deriving the above equations: (1) at room temperature, change of DE's elastic modulus is small [40], and is regarded as a constant for the convenience of analysis; (2) the MBDEA deforms uniformly and the induced curvature stays constant on the bending curve of the entire actuator; (3) the section is still plane after deformation; (4) the radius of curvature is very large relative to the MBDEA's thickness.

C. *Modeling of MESDEAs*

1) *Working principle of MESDEAs*

The MESDEA is composed of a DE film with compliant electrodes covering on both sides (the active layer), two stiffeners and one elastic frame. The structure is shown in Fig. 4(a). First, we biaxially pre-stretch the DE film, and apply compliant electrodes to both sides of the film according to the hollow area's shape, then we paste the elastic frame and stiffeners on different sides of the film. Fig. 4(b) shows the completed MESDEA. Part of the pre-stretched film's strain energy is converted into the elastic frame's bending energy. The MESDEA eventually settles at the minimum energy state. And the MESDEA folds only about the y-axis because the stiffeners increase its bending stiffness about the x-axis. When the electrodes are powered on, the film will compress in thickness and extend in plane. It will offset some of the internal stress of the pre-stretched film, thereby breaking the current equilibrium state of the MESDEA. As shown in Fig. 4(b), the MESDEA will fold a certain angle about the y-axis toward plane direction because of the bending moment of elastic frame and stabilize in another equilibrium state.

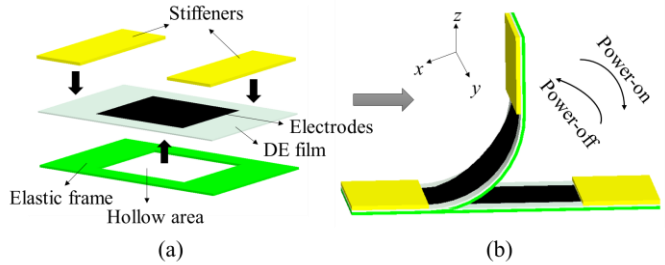

Fig. 4. The MESDEA's structure and working principle.

2) *Design Model of MESDEAs*

According to the MESDEA's working principle, different from MBDEA, the angle of the MESDEA at the initial equilibrium state is the maximum deformation angle. And in the initial state, if a voltage is applied to release the internal stress of the pre-stretched DE, the maximum output moment of MESDEA is the restoring moment of the elastic frame. The maximum deformation angle and maximum output moment of the MESDEA are two basic indicators, and are both determined by its initial state. Therefore, it is necessary to propose a design model for the initial state of the MESDEA.

The MESDEA's structural dimensions are shown in Fig. 5, and the shape of the elastic frame's hollow area is rectangular. When MESDEA is in equilibrium, the film's moment M_{film} to elastic frame is equal to the elastic frame's bending moment

M_{frame}. Due to the viscoelasticity and hyperelasticity of DE and the special saddle surface formed by the film, its moment at different deformation angles θ cannot be directly expressed analytically when the MESDEA does not reach the equilibrium state. However,

$$M(\theta) = M_{film}(\theta) + M_{frame}(\theta) \tag{11}$$

where $M(\theta)$ is the MESDEA's output moment at different deformation angles. To obtain $M_{film}(\theta)$, we can use the equivalent moment calibration method [41] to measure $M(\theta)$ and the elastic frame's bending moment $M_{frame}(\theta)$. $M(\theta)$ is measured during the change of MESDEA from the planar state to the bending equilibrium state. $M_{frame}(\theta)$ is measured during the change from the bending state to the planar state after removing the DE film in the hollow area. In this way, we can get $M_{film}(\theta)$ through (11). When MESDEA is in equilibrium, the elastic frame's bending moment is also equal to the DE film's moment to the elastic frame, which is,

$$M_{max} = M_{frame}(\theta_e) = M_{film}(\theta_e) \tag{12}$$

where M_{max} is the maximum output moment and θ_e is the equilibrium angle of the MESDEA.

In addition, for MESDEAs, with the same deformation angle, pre-stretch ratio and hollow area shape, the ratio of DE film's moment to its volume in hollow area is constant [38], that is,

$$M_{film} = kV_{film} \tag{13}$$

$$V_{film} = lbh = lbnh_{film} \tag{14}$$

where k is a constant, V_{film} is the volume of DE films in the elastic frame's hollow area, n is the number of films' layers, and h_{film} is one-layer pre-stretched film's thickness. According to (15), if $M_{film-1}(\theta)$ and V_{film-1} of a MESDEA are known, the V_{film-2} of another MESDEA with the equilibrium deformation angle of θ_2 and the maximum output moment of M_{max-2} can be calculated, and then other size parameters of the MESDEA can be designed.

$$\frac{M_{film-1}(\theta_2)}{M_{max-2}} = \frac{M_{film-1}(\theta_2)}{M_{film-2}(\theta_2)} = \frac{V_{film-1}}{V_{film-2}} \tag{15}$$

Now, a sample MESDEA is selected and its $M_{film-s}(\theta)$, l_s, b_s and n_s are recorded. We intend to design a MESDEA whose equilibrium deformation angle is θ_d and the maximum output moment is $M_{max-d} = M_{frame-d}(\theta_d) = M_{film-d}(\theta_d)$. According to (13) and (14):

$$\frac{M_{max-d}}{M_{film-s}(\theta_d)} = \frac{V_d}{V_s} = \frac{l_d}{l_s} \cdot \frac{b_d}{b_s} \cdot \frac{n_d}{n_s} \tag{16}$$

The subscript 's' represents the parameters of the sample MESDEA, while the subscript 'd' represents the parameters of the designed MESDEA. Therefore, we can design the MESDEA's l_d, b_d and n_d through (16). Besides, the elastic frame's bending moment at different folding angles θ is:

$$M_{frame}(\theta) = \frac{E(w-b)t^3\theta}{12l} \tag{17}$$

where E is the elastic frame's elastic modulus. When the designed MESDEA is at initial equilibrium deformation angle,

$$M_{max-d} = M_{frame-d}(\theta_d) = \frac{E(w_d-b_d)t_d{}^3\theta_d}{12l_d} \tag{18}$$

Determine t_d according to optional elastic frames, and then calculate w_d by (18). The elastic frame's length L_d and stiffeners' thickness s_d do not affect the designed MESDEA's θ_d and M_{max-d}, so we can determine the two parameters according to actual requirements. Thus far, all of the designed MESDEA's parameters (l_d, b_d, n_d, t_d, w_d, s_d and L_d) are determined. With these parameters, the MESDEA whose equilibrium deformation angle is θ_d and the maximum output moment is M_{max-d} can be fabricated. In summary, with a sample MESDEA's V_{film} and $M_{film}(\theta)$, the MESDEA that meets the required indicators (the equilibrium deformation angle θ_e and maximum output moment M_{max}) can be designed.

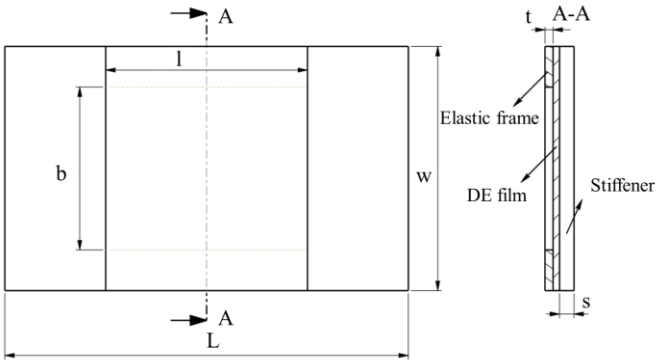

L: the elastic frame's length; w: the elastic frame's width; t: the elastic frame's thickness; s: the stiffener's thickness; l: the hollow area's length; b: the hollow area's width.

Fig. 5. The MESDEA's structural dimensions.

III. Experiments and Results

A. Effects of Design Parameters Inferred from MBDEA's Model

We intend to first investigate the effect of the number of active layers on MBDEA's deformation angle and output moment through the analytical model. Select VHB F9473PC coated with compliant electrodes on both sides as the active layer, VHB F9473PC without coated electrodes as the passive layer, and carbon grease as the compliant electrodes. The design parameters of the MBDEA are shown in Table I. The relationship between the MBDEA's deformation angle θ, output moment M and input electric field intensity E obtained from (8) and (9) are shown in Fig. 6.

TABLE I
Design Parameters of the MBDEA

Description	Symbol	Value
Number of active layers	n	1, 3, 9
Thickness ratio of the passive layer to the active layer	α	1
Ratio of elastic modulus of the passive layer to the active layer	β	1
Electrostrictive coefficient of DE	M_a	4.16×10^{-17} m^2/V^2
Thickness of DE	t_a	0.26 mm
Elastic modulus of DE	Y_a	0.5 MPa [40]
Length of the MBDEA	L	20 mm
Width of the MBDEA	b	15 mm

Fig. 6 shows that as the number of active layers increases, the deformation angle of the MBDEA decreases while the output moment increases. And both the deformation angle and output moment are nonlinear with the electric field intensity. In addition, according to (8), the deformation angle of the

MBDEA is proportional to its length; according to (9), the output moment of the MBDEA is proportional to its width.

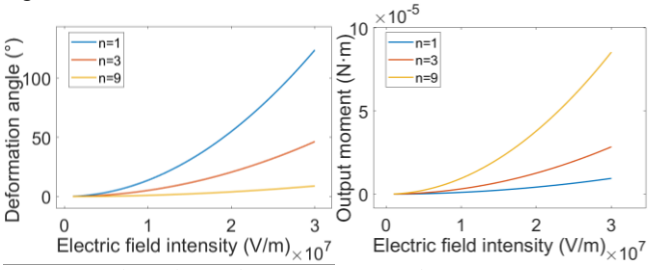

(a) Deformation angle (b) Output moment

Fig. 6. MBDEA's analytical curve.

B. Experimental Exploration of MBDEAs

We only explore the deformation of MBDEAs in this letter. From (7) and (8), it can be known that after materials are determined, the deformation angle of MBDEA is related to the number of active layers n, length L and electric field intensity E. When the active layers' number and length of the MBDEA are 3 and 36 mm, and two pieces of paper with length of 15 mm are pasted on one side to ensure the MBDEA only folds along the length direction at the crease. Then the crease's length is 6 mm, which is L in the analytical model. Through extensive experiments, we find that VHB F9473PC is broken down when the electric field intensity is approximately 29 MV/m. Then we set the range of electric field intensity within 27 MV/m. The experimental data and analytical curve are shown in Fig. 7(a). In addition, when n=1 and the crease's lengths are 3 mm and 6 mm respectively, the experimental and analytical results are shown in Fig. 7(b) and (c); when n=2 and the crease's length is 10 mm, the results are shown in Fig. 7(d).

Comparing Fig. 7(a) and (c), it can be seen that the folding angle of the MBDEA decreases as n increases. From Fig. 7(b) and (c), the folding angle increases as L increases and the relationship is almost linear. The effects of n and L on the folding angle of the MBDEA are consistent with the analysis. In addition, comparing Fig. 7(c) and (d), shows that the experimental results and analytical curves of the two MBDEAs are close. This is because although the n of the MBDEA in Fig. 7(d) is twice that of the MBDEA in Fig. 7(c), its L is 1.67 times that of the MBDEA in Fig. 7(c). The effect of decreasing folding angle caused by increasing the number of active layers is offset by increasing length. Besides, the error between experimental data and analytical curve is small when the intensity of electric field is low, and gradually increases when the electric field intensity increases. This is because in the derivation of the analytical model, it is assumed that the stress-strain relationship of DE is linear, but in fact, when MBDEA gradually bends, the strain of DE increases and its elastic modulus Y_a decreases [42]. According to (4), (7) and (8), the decrease in Y_a leads to an increase in M_a, which in turn leads to an increase in κ and θ. Moreover, in the bending of MBDEA, from (7) and (8), the decrease in DE's thickness t_a and increase in length L also lead to the increase in θ. All these aspects cause the angle error to increase with increasing input electric field intensity.

Then, the MBDEAs whose n=3, L=6 mm are used to drive the origami-inspired robot joint. Based on the deformation characteristic of MBDEAs, they are placed on the four creases between the pentagonal sheets and the triangular sheets of one leg. Fig. 7(e) shows the change of the origami folding hinge after MBDEAs are powered on. When the driving voltage is 7 kV, that is, the input electric field intensity is 27 MV/m, the angle change of the origami folding hinge is 4°. However, Fig. 7(a) shows that the same MBDEA's folding angle is 25° with an input electric field intensity of 27 MV/m, which is much larger than it is in the joint. This is because the output moment of MBDEAs is too small to overcome the folding resistance created at the creases when the joint bends.

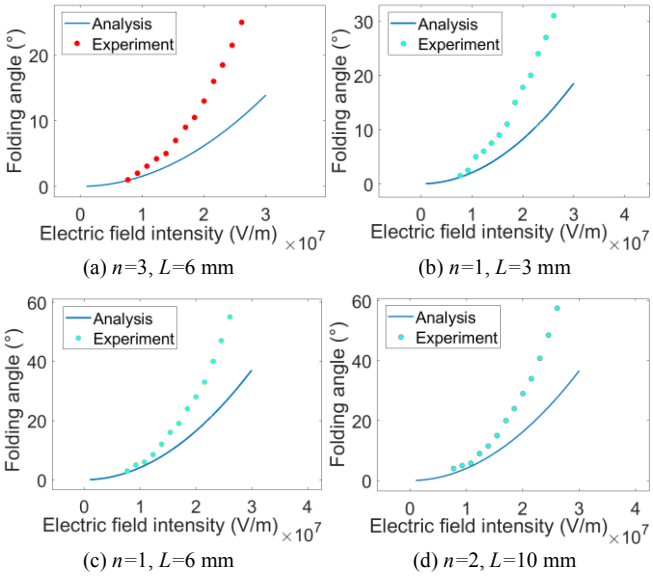

(a) n=3, L=6 mm (b) n=1, L=3 mm

(c) n=1, L=6 mm (d) n=2, L=10 mm

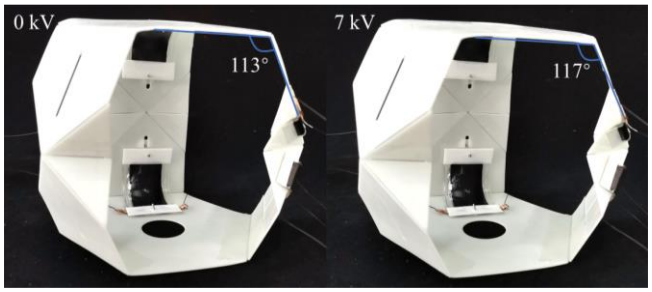

(e)

Fig. 7. Experiments of the MBDEA and origami-inspired robot joint. (a-d) Comparisons of experimental data and analytical curves. (e) Drive of the origami-inspired robot joint.

C. Experimental Exploration of MESDEAs

In the experiments of MESDEAs, VHB 4910 is selected as DE, carbon greases are selected as compliant electrodes, PET is used as the elastic frame, and stiffeners are made by 3D printing. To verify the design model in Section II *C*, a sample MESDEA (Fig. 8(a)) is selected and its parameters are shown in Table II. We intend to design a MESDEA whose equilibrium deformation angle is 90° and its maximum output moment is about twice the sample MESDEA's. We first take b_d, l_d and n_d as 20 mm, 35 mm and 3, then,

$$\frac{M_{max-d}}{M_{max-s}} = \frac{M_{frame-d}(\theta_d)}{M_{frame-s}(\theta_s)} = \frac{M_{film-d}(\theta_d)}{M_{film-s}(\theta_s)} = \frac{M_{film-d}(90°)}{M_{film-s}(90°)} = \frac{V_d}{V_s} = \frac{l_d}{l_s} \cdot \frac{b_d}{b_s} \cdot \frac{n_d}{n_s} = 2.1 \quad (21)$$

The designed MESDEA's maximum output moment is 2.1 times the sample MESDEA's. When the sample and designed MESDEAs are at initial equilibrium deformation angles,

$$\frac{E(w_d-b_d){t_d}^3\theta_d}{12l_d} = 2.1 \times \frac{E(w_s-b_s){t_s}^3\theta_s}{12l_s} \tag{22}$$

which is,

$$\frac{(w_d-20){t_d}^3}{35} = 0.0049 \tag{23}$$

TABLE II
THE SAMPLE AND DESIGNED MESDEAS' PARAMETERS

The sample MESDEA		The designed MESDEA	
Pre-stretch ratio	400%×200%	Pre-stretch ratio	400%×200%
θ_s	90°	θ_d	90°
W_s	30 mm	W_d	30 mm
t_s	0.18 mm	t_d	0.26 mm
l_s	25 mm	l_d	35 mm
b_s	20 mm	b_d	20 mm
n_s	2	n_d	3
L_s	50 mm	L_d	55 mm
s_s	0.7 mm	s_d	0.7 mm

There are optional PET sheets whose thickness is 0.26 mm, so take $t_d = 0.26$ mm and is substituted into (23) to get $w_d = 29.76$ mm. Then we take $w_d = 30$ mm for the convenience of fabrication. As a result, $M_{frame-d}/M_{frame-s} = 2.15$, and the error is only 2.38% compared to the expected ratio of 2.1. The final designed MESDEA's parameters are shown in Table II, and its initial deformation angle is shown in Fig. 8(b). As seen from Fig. 8, with the design model in Section II *C*, the designed MESDEA's initial deformation angle (right) is also 90°, which is the same as that of the sample MESDEA (left), meeting the expected purpose.

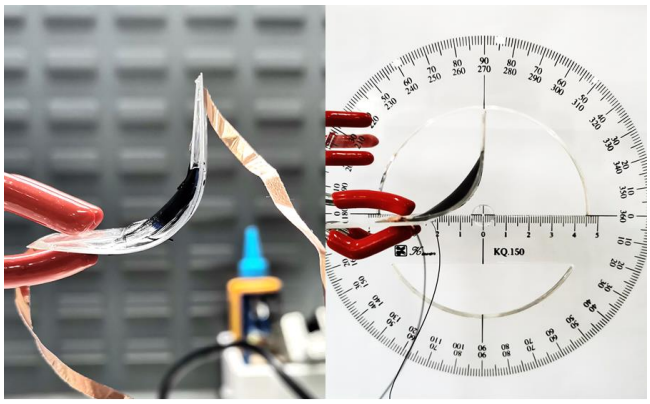

(a) The sample MESDEA (b) The designed MESDEA

Fig. 8. The initial deformation angles of two MESDEAs.

On the other hand, it is necessary to explore its electrodeformability for driving origami-inspired robots. Also due to the viscoelasticity and hyperelasticity of DE and its special saddle surface shape, the analytical expression for MESDEA's angle θ and its driving voltage V cannot be given. Therefore, we obtain $\theta(V)$ by fitting experimental results. The folding angles of the designed MESDEA at different driving voltage and its fitting curve are shown in Fig. 9(a). The MESDEA has a maximum angle change of 60° at a driving voltage of 5.4 kV. We think that with the pre-stretch ratio of 400% × 200%, DE has already the maximized stress relief at 5.4 kV, and increasing the driving voltage cannot further relieve the stress on the length. Therefore, when the driving voltage is 5.4 kV, the moment of DE to the elastic frame is the smallest, and the output moment of the MESDEA is the largest.

Finally, we use the designed MESDEA to drive the origami-inspired robot joint. Based on MESDEAs' deformation characteristic, we put two MESDEAs on the creases of the origami folding hinges. Note that the leg used this time is different from that used before. Fig. 9(b) shows the angle change of the origami folding hinge when MESDEAs are powered on. When the input voltage is 5.4 kV, the origami folding hinge's angle change is 23°. Likewise, Fig. 9(a) shows that the angle of the MESDEA changes by 60° at 5.4 kV, which is larger than it is in the joint. This is also due to the MESDEAs' insufficient output moment.

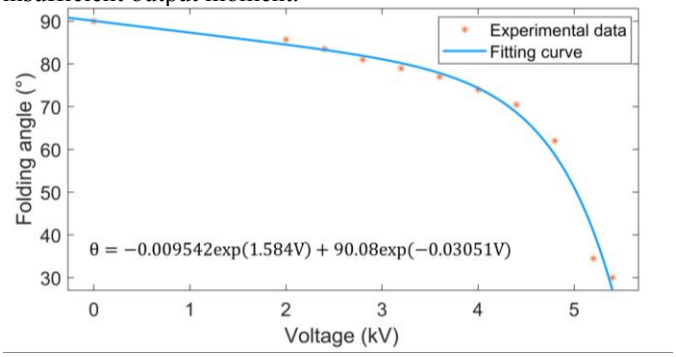

(a)

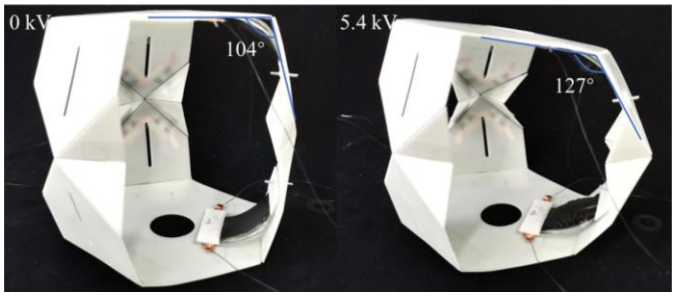

(b)

Fig. 9. Experiments of the MESDEA and origami-inspired robot joint. (a) The folding angles of the MESDEA at different driving voltage and its fitting curve. (b) Drive of the origami-inspired robot joint.

IV. DISCUSSION

In light and small origami-inspired robots, it will be an inevitable trend to apply smart materials to drive them. Ahmed *et al*. [30] used MBDEAs for the first time to achieve simple actions of paper-based origami structures, namely close of the crocodile jaw and conversion of two stable shapes of the water bomb. However, there have been no studies applying DEAs to origami structures since then. In this letter, we integrate not only MBDEAs, but also MESDEAs for the first time to drive a rigid origami-inspired robot joint, proving the application prospects of DEAs in driving origami-inspired robots. Through analysis and experimentation, MBDEAs and MESDEAs that meet the deformation requirements for origami-inspired robots are designed. The angle changes of both DEAs after power-on can be greater than 60°, meeting the basic folding requirements of most origami-inspired robots. In addition, the MBDEA's

deformation characteristic is from straight to folding, while it is from folding to straight for the MESDEA. Therefore, their folding occasions are opposite and complementary. In subsequent driving experiments of the origami-inspired robot joint, the angle changes of the origami folding hinges driven by the two DEAs are not large, indicating that both DEAs' moments are insufficient. However, both DEAs can increase their output moments by increasing the active layers' number and optimizing the size, while ensuring their folding angles roughly unchanged. The MBDEA can increase its output moment by increasing the number of layers and width of DE films, and their effect of reducing the deformation angle can be counteracted by increasing the length of the crease; the MESDEA can improve its moment by increasing the volume of pre-stretched DE in hollow area, also its effect of increasing its initial equilibrium angle can be counteracted by increasing the elastic frame's width and thickness. In addition, four MBDEAs can only change the origami folding hinge by a maximum of 4°, while two MESDEAs can change it by a maximum of 23°, showing that the driving force of MESDEAs is much greater than that of MBDEAs. Therefore, MBDEAs are more suitable for driving light and small origami-inspired robots made of flexible materials such as paper, and MESDEAs can be applied to stiff origami-inspired robots.

On the other hand, there are relatively few publications about the design methods of MBDEAs and MESDEAs. Energy density equations of hyperelastic materials are used in [34]-[37] to characterize DE's constitutive behaviors for modeling MBDEAs or MESDEAs. Uniaxial or biaxial tensile experiments are required to fit the parameters in energy density equations. However, the tensile force is related to its loading time due to DE material's viscoelasticity. Therefore, energy density equations determined by tensile experiments generally cannot actually describe the characteristics of DE. Ahmed *et al.* [18] developed sets of nondimensional expressions for curvature, displacement at the tip and blocked force induced by the electric field to guide the design and fabrication of multilayered EAP actuators, and used P(VDF–TrFE–CTFE) to verify the model by experiments. However, their actuators and model contain adhesive layers, which are more complicated to fabricate and analyze. The analytical model established in this letter is based on beam bending theory and neither uses any energy density equation nor needs to consider the effect of adhesive layers because of the stickiness of DE film itself. The parameters of DE used in the model such as the elastic modulus and thickness can directly refer to the official data of 3 M company. Therefore, the fabrication and analytical model of MBDEAs are simple to implement. For MESDEAs, there are two commonly used hollow areas, namely rectangular and double semicircular. Wang *et al.* [38] presented a design method for MESDEAs with the double semicircular hollow area. Actually, when the lengths, widths of the hollow area and numbers of DE layers are equal, the output moment of the MESDEA with rectangular one is larger. Therefore, this letter proposes a design model for MESDEAs with the rectangular hollow area, which is simple and practical. The model also does not need any energy density equation and only needs one sample MESDEA to implement, and the sample MESDEA can be homemade or selected from published studies. It should be noted that the MBDEA's model is used to analyze changes of its deformation angle and output moment under the electric field, while the MESDEA's model is for the design of its initial state after fabrication to obtain the equilibrium deformation angle and maximum output moment. Both models can guide the experimental design and fabrication of MBDEAs or MESDEAs.

It is necessary to summarize some limitations of the current work and point out future research directions. First, the ideal angle change of the origami folding hinge is at least 60°, but it is only 23° here, indicating that the current output moment of MESDEAs is small. According to the model in this letter, we will continue to optimize the design of MESDEAs to meet the deformation requirements of origami-inspired robots. Limited by their small driving force, MBDEAs are suitable for driving origami-inspired robots made of flexible materials such as paper. Second, the experiments mainly focus on the quasi-static deformation of both DEAs and do not verify their output moment in the models. And without $M_{film-s}(\theta)$ of the sample MESDEA, only MESDEAs with the same equilibrium deformation angle as the sample can be designed. DEA's output moment and dynamic characteristics need to be studied for future control of origami-inspired robots. Finally, this letter only selects one origami-inspired robot for bending experiments to preliminarily verify the prospect of DEAs in the driving field of origami-inspired robots. We hope to combine DEAs with different origami structures to make versatile origami-inspired robots for more practical scenarios in the future.

V. Conclusion

In this letter, we model and characterize two dielectric elastomer folding actuators and provide a new method for driving origami-inspired robots. MBDEAs and MESDEAs are integrated for the first time into a rigid origami-inspired robot joint to drive folding hinges. We explore the factors that affect the performances of the two DEAs and present their models. Using MBDEA's analytical model, its deformation angle and output moment at different electric field intensities can be obtained according to the design parameters (the number of layers of DE, the length and width of the MBDEA). Through MESDEA's design model, we can design the MESDEA with different initial deformation angles or maximum output moments with one sample MESDEA. Based on our models, corresponding DEAs can be designed according to the folding requirements (deformation angle and driving moment) of different origami-inspired robots. The driving experiments of the origami-inspired robot joint show that the origami folding hinge driven by MBDEAs changes by 4° with an input voltage of 7 kV, while the other origami folding hinge driven by MESDEAs changes by 23° with an input voltage of 5.4 kV, proving that DEAs have great prospects in driving origami-inspired robots. Also, DEA-driven origami-inspired robots may further expand their applications.

References

[1] D. Rus and M. T. Tolley, "Design, fabrication and control of origami robots," *Nature Reviews. Materials,* vol. 3, no. 6, pp. 101-112, 2018.

[2] C. H. Belke and J. Paik, "Mori: A Modular Origami Robot," *IEEE/ASME Transactions on Mechatronics,* vol. 22, no. 5, pp. 2153-2164, 2017.

[3] H. Zhang *et al*, "Generalized modeling of origami folding joints," *Extreme Mechanics Letters,* vol. 45, pp. 101213, 2021.

[4] C. Liu *et al*, "A Self-Folding Pneumatic Piston for Mechanically Robust Origami Robots," *IEEE Robotics and Automation Letters,* vol. 4, no. 2, pp. 1372-1378, 2019.

[5] M. A. Robertson, O. C. Kara, and J. Paik, "Soft pneumatic actuator-driven origami-inspired modular robotic "pneumagami"," *The International Journal of Robotics Research*, p. 0278364920909905, 2020.

[6] H. Yang *et al*, "Multifunctional metallic backbones for origami robotics with strain sensing and wireless communication capabilities," *Science Robotics*, vol. 4, no. 33, pp. 1–14, 2019.

[7] S. Liu *et al,* "Otariidae-Inspired Soft-Robotic Supernumerary Flippers by Fabric Kirigami and Origami," *IEEE/ASME Transactions on Mechatronics,* vol. 26, no. 5, pp. 2747-2757, 2021.

[8] S. Miyashita, S. Guitron, S. Li, and D. Rus, "Robotic metamorphosis by origami exoskeletons," *Science Robotics*, *2*(10), eaao4369, 2017.

[9] R. Swaminathan *et al*, "Multiphysics Simulation of Magnetically Actuated Robotic Origami Worms," *IEEE Robotics and Automation Letters,* vol. 6, no. 3, pp. 4923-4930, 2021.

[10] D. Tang *et al*, "Origami-inspired magnetic-driven soft actuators with programmable designs and multiple applications," *Nano Energy,* vol. 89, pp. 106424, 2021.

[11] S. Wu *et al*, "Stretchable origami robotic arm with omnidirectional bending and twisting," *Proceedings of the National Academy of Sciences - PNAS,* vol. 118, no. 36, pp. 1, 2021.

[12] Y. Sun, Y. Jiang, H. Yang, L.-C. Walter, J. Santoso, E. H. Skorina, and C. Onal, "Salamanderbot: A soft-rigid composite continuum mobile robot to traverse complex environments," *2020 IEEE International Conference on Robotics and Automation (ICRA)*, May 2020, pp. 2953– 2959.

[13] K. Lee, Y. Wang and C. Zheng, "TWISTER Hand: Underactuated Robotic Gripper Inspired by Origami Twisted Tower," *IEEE Transactions on Robotics,* vol. 36, no. 2, pp. 488-500, 2020.

[14] Z. Zhang *et al*, "A Pneumatic/Cable-Driven Hybrid Linear Actuator With Combined Structure of Origami Chambers and Deployable Mechanism," *IEEE Robotics and Automation Letters,* vol. 5, no. 2, pp. 3564-3571, 2020.

[15] J. Santoso and C. D. Onal, "An Origami Continuum Robot Capable of Precise Motion Through Torsionally Stiff Body and Smooth Inverse Kinematics," *Soft Robotics,* vol. 8, no. 4, pp. 371, 2021.

[16] S. Felton *et al*, "A method for building self-folding machines," *Science (American Association for the Advancement of Science),* vol. 345, no. 6197, pp. 644-646, 2014.

[17] C. D. Onal, R. J. Wood and D. Rus, "An Origami-Inspired Approach to Worm Robots," *IEEE/ASME Transactions on Mechatronics,* vol. 18, no. 2, pp. 430-438, 2013.

[18] S. Ahmed, Z. Ounaies and E. A. F. Arrojado, "Electric field-induced bending and folding of polymer sheets," *Sensors and Actuators. A. Physical,* vol. 260, pp. 68-80, 2017.

[19] H. Okuzaki *et al*, "Humidity-Sensitive Polypyrrole Films for Electro-Active Polymer Actuators," *Advanced Functional Materials,* vol. 23; 10;, no. 6;36;, pp. 4400-4407, 2013.

[20] K. W. Kwan, S. J. Li, N. Y. Hau, W. D. Li, S. P. Feng, and A. H. Ngan, "Light-stimulated actuators based on nickel hydroxide-oxyhydroxide," *Science Robotics*, *3*(18), eaat4051, 2018.

[21] P. Brochu and Q. Pei, "Advances in Dielectric Elastomers for Actuators and Artificial Muscles," *Macromolecular Rapid Communications,* vol. 31, no. 1, pp. 10-36, 2010.

[22] K. McGough *et al*, "Finite element analysis and validation of dielectric elastomer actuators used for active origami," *Smart Materials and Structures,* vol. 23, no. 9, pp. 94002, 2014.

[23] F. Chen *et al*, "An Integrated Design and Fabrication Strategy for Planar Soft Dielectric Elastomer Actuators," *IEEE/ASME Transactions on Mechatronics,* vol. 26, no. 5, pp. 2629-2640, 2021.

[24] H. Godaba *et al*, "A Soft Jellyfish Robot Driven by a Dielectric Elastomer Actuator," *IEEE Robotics and Automation Letters,* vol. 1, no. 2, pp. 624-631, 2016.

[25] N. Wang *et al*, "Design of dielectric elastomer grippers using Bezier curves," *Mechanism and Machine Theory,* vol. 158, 2021.

[26] G. Kovacs *et al*, "Stacked dielectric elastomer actuator for tensile force transmission," *Sensors and Actuators. A. Physical,* vol. 155, no. 2, pp. 299-307, 2009.

[27] N. Liu *et al*, "Control-Oriented Modeling and Analysis of Tubular Dielectric Elastomer Actuators Dedicated to Cardiac Assist Devices," *IEEE Robotics and Automation Letters,* vol. 7, *(2),* pp. 4361-4367, 2022.

[28] J. Shintake *et al*, "A Foldable Antagonistic Actuator," *IEEE/ASME Transactions on Mechatronics,* vol. 20, no. 5, pp. 1997-2008, 2015.

[29] J. Li, L. Liu, Y. Liu, *et al,* "Dielectric Elastomer Spring-Roll Bending Actuators: Applications in Soft Robotics and Design," *Soft Robotics,* 2018.

[30] S. Ahmed, Z. Ounaies and M. Frecker, "Investigating the performance and properties of dielectric elastomer actuators as a potential means to actuate origami structures," *Smart Materials and Structures,* vol. 23, no. 9, pp. 94003, 2014.

[31] J. Zhao *et al*, "Phenomena of nonlinear oscillation and special resonance of a dielectric elastomer minimum energy structure rotary joint," *Applied Physics Letters,* vol. 106, no. 13, pp. 133504, 2015.

[32] D. L. DeVoe and A. P. Pisano, "Modeling and optimal design of piezoelectric cantilever microactuators," *Journal of Microelectromechanical Systems,* vol. 6, no. 3, pp. 266-270, 1997.

[33] B. Balakrisnan, A. Nacev and E. Smela, "Design of bending multi-layer electroactive polymer actuators," *Smart Materials and Structures,* vol. 24, no. 4, pp. 45032, 2015.

[34] K. Luo, Q. Tian and H. Hu, "Dynamic modeling, simulation and design of smart membrane systems driven by soft actuators of multilayer dielectric elastomers," *Nonlinear Dynamics,* vol. 102, no. 3, pp. 1463-1483, 2020.

[35] B. O'Brien *et al*, "Finite element modelling of dielectric elastomer minimum energy structures," *Applied Physics A,* vol. 94, no. 3, pp. 507-514, 2008; 2009;.

[36] B. O'Brien *et al*, "FEA of dielectric elastomer minimum energy structures as a tool for biomimetic design," *Proc. SPIE.* 2009, 7287 728706.

[37] S. Rosset *et al*, "Model and design of dielectric elastomer minimum energy structures," *Smart Materials and Structures,* vol. 23, no. 8, pp. 85021, 2014.

[38] S. Wang *et al*, "Design method of DEMES rotary joint," *Smart Materials and Structures,* vol. 29, no. 3, pp. 35021, 2020.

[39] Z. Cheng, V. Bharti, T. Xu, H. Xu, T. Mai, Q.M. Zhang, "Electrostrictive poly (vinylidene fluoride-trifluoroethylene) copolymers," *Sensors and Actuators. A. Physical,* 90, 138–147, 2001.

[40] G. Lau, S. C. Goh and L. Shiau, "Dielectric elastomer unimorph using flexible electrodes of electrolessly deposited (ELD) silver," *Sensors and Actuators. A. Physical,* vol. 169, no.1, pp. 234-241, 2011.

[41] J. Zhao *et al*, "Equivalent dynamic model of DEMES rotary joint," *Smart Materials and Structures,* vol. 25, no. 7, pp. 75025, 2016.

[42] M. Wissler and E. Mazza, "Mechanical behavior of an acrylic elastomer used in dielectric elastomer actuators." *Sensors and Actuators. A. Physical,* vol.134 no.2, pp. 494-504, 2007.